Laser Detection of Thermal Flows: An Analytical Model and Experimental Investigation

Gregory Dolya

V. N. Karazin Kharkiv National University, Kharkiv, Ukraine

DOI: https://doi.org/10.68050/JAMS.2026.903

Received: 20 October 2026; Accepted: 28 October 2026; Published: 02 November 2026

ABSTRACT

This paper presents an analytical model for laser detection of thermal flows based on recording temporal fluctuations in the total power of coherent radiation after it interacts with temperature inhomogeneities in air. The model links the spatiotemporal correlation of refractive-index fluctuations to the measured photocurrent spectrum. It accounts for the two-pass optical geometry, the lateral offset of the photodetector, the finite receiving aperture, anisotropy in the spatial structure of the inhomogeneities, and possible changes in their intensity with distance from the heat source.

Experiments were conducted using a hair dryer as the thermal-flow source. Horizontal and vertical geometries were investigated, together with several positions of the interaction region along the optical path and fan-to-beam distances ranging from 2 to 40 cm. Photocurrent spectra were obtained by averaging spectral estimates over selected informative intervals of the recordings.

The study establishes an analytical relationship between the statistical properties of thermal inhomogeneities, the optical-system geometry, and the recorded photocurrent spectrum. The experimental results are used for a preliminary qualitative comparison with the model. The attenuation parameters and spatial correlation scales have not been determined from the available measurements.

Keywords: laser detection of thermal flows, temperature inhomogeneities, refractive index of air, coherent radiation, phase fluctuations, photocurrent spectrum, anisotropy, spatial correlation, two-pass optical arrangement.

1. INTRODUCTION

Laser remote-sensing techniques are widely used in many applied and engineering fields [1, 2]. Their principal advantage is that they are non-invasive: unlike contact sensors, they do not disturb the object being investigated. One application is the laser diagnosis of gas and liquid jets, flows, and plasma through the interaction of laser radiation with matter, including scattering, absorption, fluorescence, and refraction [3, 4].

Temperature inhomogeneities in air produce refractive-index fluctuations and thus perturb the phase of a propagating optical field. Depending on the detection geometry, these perturbations can change the beam position, the intensity distribution, and the total optical power reaching the photodetector. The effects of random inhomogeneities on laser-beam propagation have been studied extensively in atmospheric optics and optical communications [5–7].

In the method considered here, a laser beam traverses a region of heated air, interacts with a retroreflective surface, and returns to the photodetector. The measured signal is the time-dependent photocurrent; its informative characteristics include the power spectral density and correlation properties. Related configurations have previously been used to detect heat sources along a laser-beam path and to detect acoustic waves [8, 9].

Signal formation involves several coupled factors: the spatial distribution of temperature fluctuations; the rel-

ationship between temperature and the refractive index of air; transport and temporal evolution of the inhomogeneities; propagation of the coherent field along the forward and return paths; interference between optical contributions; and the finite receiving aperture and lateral offset of the photodetector.

The orientation of the thermal flow relative to the optical system is particularly important. If the inhomogeneities have an anisotropic spatial structure, changing their transport direction can alter the temporal photocurrent spectrum even when the temperature-fluctuation levels are comparable.

Another feature of the setup is that the forward and return beams pass through the thermal-flow region along different trajectories. Their phase perturbations may therefore be correlated or partly independent. The effects of correlations between separated optical paths are also known in other problems involving propagation through random media [5].

The aim of this study is to develop an analytical description of photocurrent-spectrum formation in a two-pass laser system and to compare the model's qualitative predictions with experiments for horizontal and vertical thermal-flow geometries. Rather than providing only a phenomenological description, the approach relates the measured spectrum to the spatiotemporal correlation of refractive-index fluctuations and to the optical sensitivity of the setup. The assumptions are treated as hypotheses to be tested, not as properties of the thermal flow established in advance.

2. METHODOLOGY

2.1 Experimental setup

Optical geometry

The experimental setup is shown in Fig. 1.

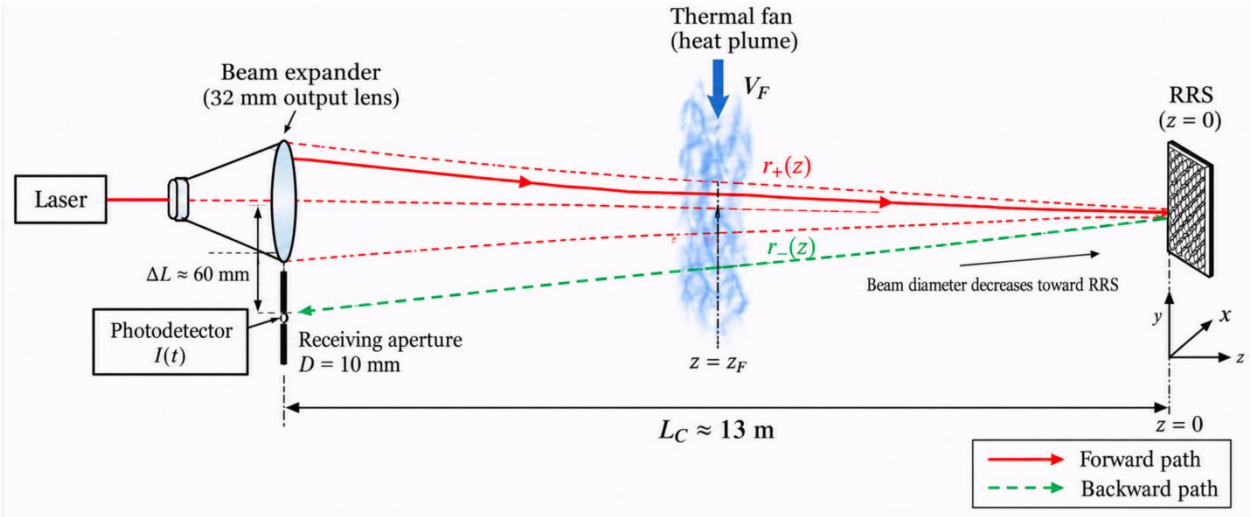


Figure 1. Experimental setup for laser detection of a thermal flow.

Laser radiation at a wavelength of 532 nm is expanded by an optical system with a 32 mm output lens and directed toward a retroreflective surface (RRS). The distance from the optical assembly to the RRS is approximately 13 m.

The returning radiation is detected by a photomultiplier tube (PMT) displaced laterally from the axis of the outgoing beam. A diaphragm with a diameter of 10 mm defines the receiving aperture. The transverse offset, $\Delta L \approx 60$ mm, is the distance between the centre of the diaphragm and the axis of the outgoing laser beam. The PMT was connected to a load circuit that enabled its signal to be recorded using a sound card.

The RRS consists of glass microspheres with a mean diameter of approximately 50 μm and a packing fraction of about 70%. These parameters describe the retroreflective surface but are not, by themselves, sufficient to determine the reflectance of the complete optical system.

A hair dryer was used to generate the thermal flow. The distance d between the hair dryer and the laser beam was varied (2, 5, 10, 25, and 40 cm), as was the position of the interaction region along the optical path. These are distinct parameters: d is the transverse distance from the hair dryer to the beam, whereas z denotes the nominal longitudinal position of the interaction region in the adopted experimental coordinate system.

Horizontal and vertical series

In the horizontal series, the principal transport vector of the thermal inhomogeneities is directed along one transverse axis; in the vertical series, it is directed along the other. The two series therefore differ in the orientation of the transport direction relative to the optical system.

For each geometry, the signal was studied as a function of the distance d between the hair dryer and the laser beam. The nominal distances were d = 2, 5, 10, 25, and 40 cm. Additional series were recorded for different positions of the interaction region along the optical path, including z = 0 m and z = 8 m.

In the adopted experimental coordinate system, z = 0 m corresponds to a region near the RRS. These labels must be kept consistent when comparing series: the distance d from the hair dryer to the laser beam and the coordinate z of the interaction region are different parameters.

Measured quantity

The photodetector recorded the time-dependent photocurrent I(t). Spectral characteristics were analysed over selected informative intervals of each recording. Because the photocurrent is produced by converting received optical power, it is not a direct measurement of temperature or air velocity at a particular point. Interpretation of the thermal flow therefore requires a model relating its statistical properties to the measured photocurrent spectrum.

2.2 Analytical model

Temperature fluctuations and refractive index

Let the refractive index of air be represented as the sum of a reference value, a mean change caused by the thermal field, and a random fluctuating component:

$$n(r\,|\,t) = n_0 + \delta n\left(r\right) + \delta n'(r\,|\,t).$$

Here, n_0 no is the reference refractive index, the mean $\delta n\left(r\right)$ term represents the change caused by the thermal field, and $\delta n'(r\,|\,t)$ the fluctuating term represents the random component. For small temperature deviations and approximately constant pressure, the refractive-index fluctuation can be linearized with respect to temperature:

$$\delta n'(r\,|\,t) \approx \left(\frac{\partial n}{\partial T}\right)_p \delta T'(r\,|\,t), \qquad (1)$$

where $\delta T'(r\,|\,t)$ the symbol denotes the temperature fluctuation, and the derivative is evaluated at constant pressure.

Thus, temperature inhomogeneities cause refractive-index fluctuations, which modify the phase of the propa-

gating optical field. The model assumes that the temperature deviations are sufficiently small for the dependence on temperature to be $n(T)$ linearized.

Anisotropic spatial correlation

Introduce the spatial correlation function of refractive-index fluctuations:

$$B_n(\rho|\, d) = \langle \delta n'(r\,|\,t)\delta n'(r\,|\,+\rho t)\rangle. \qquad (2)$$

Here, $\rho = (\rho_x\,|\,\rho_y)$ ρ is the transverse displacement between two d points, d is the distance from the heat source to the laser beam, and angle brackets denote statistical averaging.

For the transverse cross-section of the interaction region, we adopt an anisotropic Gaussian model:

$$B_n(\rho|\, d) = \sigma_n^2(d)\exp\left[-\frac{1}{2}\left(\frac{\rho_x^2}{\ell_x^2(d)} + \frac{\rho_y^2}{\ell_y^2(d)}\right)\right]. \qquad (3)$$

Here, $\sigma_n^2(d)$ the variance of the refractive-index fluctuations and $\ell_x(d)$ the $\ell_y(d)$ characteristic sizes of the spatial correlation cells along the two transverse directions are defined.

Equation (3) is a modelling approximation; a Gaussian correlation function is not assumed to be universal for a real thermal flow. It is used as a minimal parametric model that can represent different correlation scales along two transverse directions. In general, the correlation scales ℓx ℓ_x and ℓ_y σ_n^2 ℓy and the variance σn² may depend d on d. Such dependence may reflect the spreading of the thermal plume, air mixing, and changes in the geometry of the temperature inhomogeneities.

Transport direction

For the horizontal series, let the transverse component of the transport velocity be denoted by

$$V_{F,\perp}^{(H)} = (V_x\,|\,0),$$

and for the vertical series by

$$V_{F,\perp}^{(V)} = (0\,|\,V_y).$$

The axes x y correspond to the two transverse directions defined by the geometry of the experimental setup.

If the spatial inhomogeneities are anisotropic, changing the transport direction relative to the optical system changes the relationship between spatial scales and temporal frequencies. In the simplified model, the characteristic frequencies associated with the transport of correlation structures are of the order

$$f_{\text{char},H} \sim \frac{|V_x|}{2\pi\ell_x}, f_{\text{char},V} \sim \frac{|V_y|}{2\pi\ell_y}. \qquad (4)$$

These estimates illustrate how spatial structure can be converted into a temporal signal. They are not exact expressions for the frequency of a spectral maximum: the measured spectrum also depends on the spatial statistics of the inhomogeneities and on the optical sensitivity of the setup.

Change in fluctuation intensity with distance

As a first approximation, assume an exponential attenuation model for the root-mean-square amplitude of refractive-index fluctuations:

$$\sigma_n(d) = \sigma_{n,0} \exp\left(-\frac{d}{L_T}\right),$$

where $\sigma_{n,0}$ the parameter denotes the characteristic fluctuation amplitude at a reference distance and the other L_T parameter denotes the characteristic attenuation length.

The corresponding variance is then

$$\sigma_n^2(d) = \sigma_{n,0}^2 \exp\left(-\frac{2d}{L_T}\right). \qquad (5)$$

The exponential law is a phenomenological hypothesis to be tested, not a consequence that follows automatically from the general physics of convective heat flow. It may not apply across the entire range of distances. Changing the distance from the hair dryer may affect the fluctuation amplitude, the correlation-cell dimensions, and the transport velocity simultaneously. The model therefore does not assume a priori that every measured dependence must be monotonic.

Spatiotemporal correlation

As a first approximation, we use the frozen-transport hypothesis, according to which the spatial structure of the inhomogeneities is transported at the mean flow velocity without substantial change over the time interval considered:

$$\delta n'(r_\perp \mid t+\tau) \approx \delta n'(r_\perp \mid -V_{F,\perp}\tau t).$$

The spatiotemporal correlation of refractive-index fluctuations then takes the form

$$B_n(\rho \mid \tau \mid d) = B_n\left(\rho - V_{F,\perp}\tau \mid d\right). \qquad (6)$$

This approximation links the temporal spectrum to the spatial distribution of the inhomogeneities. It is valid only over time scales for which deformation and breakdown of the structures do not dominate their transport. The frozen-transport hypothesis does not mean that the thermal flow is actually stationary; it is an approximation for mapping spatial structure onto a time series observed at a fixed point.

Phase perturbations on the two passes

Let the Γ_+ Γ_- forward and return trajectories of the optical field through the region containing thermal inhomogeneities be denoted by the corresponding path symbols. The phase perturbation on the forward pass is defined by the integral

$$\phi_+(t) = k_0 \int_{\Gamma_+} \delta n'(r \mid t)\, ds,$$

and on the return pass by

$$\phi_-(t) = k_0 \int_{\Gamma_-} \delta n'(r \mid t)\, ds,$$

where

$$k_0 = \frac{2\pi}{\lambda}$$

is the vacuum wavenumber, λ and λ is the laser wavelength.

The forward Γ_+ and Γ_- return trajectories generally differ, so the phase perturbations accumulated on the two passes need not be identical. Their degree of correlation depends on the transverse separation between the trajectories and on the characteristic spatial scales of the inhomogeneities.

If the contributions from the two passes are represented by a single effective description, the total phase perturbation can be written as

$$\phi_{\text{eff}}(t) = \phi_+(t) + \phi_-(t).$$

This representation is valid when the signs of the phase contributions are defined consistently and their effect on the detected field can be represented by a single total phase perturbation. If the two paths have different geometries or optical weights, their contributions must in general be treated separately.

Integrated power and photocurrent

Let $E_D(r,t)$ denote the complex optical-field amplitude in the photodetector plane, and $E_D(r\,|\,t)$ let A_D be the area of the receiving A_D aperture. With the adopted field normalization, the measured optical power is

$$P_D(t) = \int_{A_D} |\, E_D(r\,|\,t)|^2\, dA. \qquad (7)$$

The integration is taken over the entire receiving aperture. No additional spatial-sensitivity weighting function is included, because spatial nonuniformity of the detector response is neglected in this model.

For a linear photodetector, the recorded current can be represented as

$$I(t) = I_{\text{dark}} + RP_D(t) + \nu(t), \qquad (8)$$

where I_{dark} is the constant (dark-current) component, R is the photodetector responsivity in A/W, and $\nu(t)$ represents the noise contribution.

Thus, the photocurrent is determined by the optical power integrated over the full receiving aperture. It does not directly measure temperature or air velocity at a single point.

Linearized response and effective sensitivity kernel

Represent the field in the photodetector plane as the sum of an unperturbed component and a small perturbation:

$$E_D(r\,|\,t) = E_0(r) + u(r\,|\,t),$$

where $E_0(r)$ is the unperturbed field in the scalar approximation and $u(r\,|\,t)$ is a small perturbation.

Substituting this expression into Eq. (7) gives

$$|E_D|^2 \approx |E_0|^2 + E_0^* u + E_0 u^* + |u|^2 .$$

For sufficiently small u perturbations, retaining only first-order terms gives

$$\delta P_D(t) \approx 2\mathrm{Re}\int E_0^*(r) u(r|t)\, dA. \qquad (9)$$

In the linear approximation, the power change can also be expressed in terms of phase perturbations in the interaction region:

$$\delta P_D(t) = \int_{A_F} J_{\mathrm{eff}}(\rho|z_F)\phi_{\mathrm{eff}}(\rho|t)\, d^2\rho. \qquad (10)$$

Here, A_F is the transverse interaction region, z_F is its longitudinal position in the adopted experimental coordinate system, and J_{eff} is the effective sensitivity kernel describing how a local phase perturbation changes the integrated optical power.

In the linear model, J_{eff} is defined as the functional derivative of the power response with respect to the phase perturbation:

$$J_{\mathrm{eff}}(\rho|z_F) = \frac{\delta P_D}{\delta \phi_{\mathrm{eff}}(\rho)}.$$

In general, the kernel depends on the geometry of the forward and return paths, the field distribution at the retroreflective surface, the finite receiving aperture, and the lateral displacement of the photodetector from the laser-beam axis.

If both passes can be represented using a single effective phase function, the kernel can be written as the sum of two linear contributions:

$$J_{\mathrm{eff}}(\rho|z_F) = J_+(\rho|z_F) + J_-(\rho|z_F). \qquad (11)$$

Here, J_+ and J_- are the forward-pass and return-pass contributions to the linear power response. Their sum does not mean that the powers of two independent fields are being added.

If the phase perturbations on the two passes differ substantially and cannot be reduced to a single effective phase function, the response must be written in separate terms:

$$\delta P_D(t) = \int_{A_F} J_+(\rho|z_F)\phi_+(\rho|t)\, d^2\rho + \int_{A_F} J_-(\rho|z_F)\phi_-(\rho|t)\, d^2\rho.$$

The linearized model is applicable when the phase perturbations are sufficiently small. For larger fluctuations, quadratic and higher-order terms in the response may become significant.

Photocurrent correlation and spectrum

Define the correlation function of optical-power fluctuations:

$$C_P(\tau) = \langle \delta P_D(t)\, \delta P_D(t+\tau) \rangle. \qquad (12)$$

Substituting Eq. (10) gives

$$C_P(\tau) = \iint_{A_F \times A_F} J_{\text{eff}}(\rho \mid z_F) J_{\text{eff}}(\rho' \mid z_F) \times B_\phi(\rho \mid \rho' \mid \tau \mid d)\, d^2\rho\, d^2\rho', \tag{13}$$

where

$$B_\phi(\rho \mid \rho' \mid \tau \mid d) = \langle \phi_{\text{eff}}(\rho \mid t) \phi_{\text{eff}}(\rho' \mid t+\tau) \rangle$$

is the spatiotemporal correlation function of the effective phase perturbations.

Under the frozen-transport hypothesis, the correlation can be expressed in terms of the spatial displacement caused by motion of the inhomogeneities:

$$B_\phi(\rho \mid \rho' \mid \tau \mid d) = B_\phi(\rho \mid -\rho' - V_{F,\perp} \tau d).$$

Equation (13) therefore relates the correlation of the integrated optical power to the spatial correlation of the phase perturbations and to the geometry of the optical system.

The two-sided power spectral density is defined as the Fourier transform of the correlation function:

$$S_P(f) = \int_{-\infty}^{\infty} C_P(\tau) e^{-i 2\pi f \tau}\, d\tau. \tag{14}$$

Here, f f is the temporal frequency, measured in hertz. With the definition used $S_P(f)$ here, it has units of W^2/Hz.

To obtain a spatial-frequency representation, define the Fourier transform of the effective kernel:

$$\tilde{J}_{\text{eff}}(k_\perp \mid z_F) = \int_{A_F} J_{\text{eff}}(\rho \mid z_F) e^{-i k_\perp \cdot \rho}\, d^2\rho.$$

Define the spatial spectrum of the phase inhomogeneities by the relation

$$B_\phi(\Delta \mid d) = \int_{R^2} W_\phi(k_\perp \mid d) e^{i k_\perp \cdot \Delta}\, d^2 k_\perp,$$

or, equivalently,

$$W_\phi(k_\perp \mid d) = \frac{1}{(2\pi)^2} \int_{R^2} B_\phi(\Delta \mid d) e^{-i k_\perp \cdot \Delta}\, d^2\Delta.$$

With these Fourier-transform conventions and for a real-valued effective kernel, Eq. (13) leads to the following expression for the power spectral density:

$$S_P(f \mid z_F \mid d) = \int_{R^2} \mid \tilde{J}_{\text{eff}}(k_\perp \mid z_F) \mid^2 W_\phi(k_\perp \mid d) \times \delta\left(f - \frac{k_\perp \cdot V_{F,\perp}}{2\pi} \right) d^2 k_\perp. \tag{15}$$

The sign in the argument of the delta function depends on the sign convention used for the spatiotemporal correlation and the Fourier transform. The sign shown here follows the transport representation used in deriving Eq. (15). A consistent reversal of the spatial-coordinate convention gives an equivalent expression.

Equation (15) is the central result of the analytical model. It relates the spectrum of the integrated optical power to the spatial statistics of phase inhomogeneities, their transport velocity, and the spatial sensitivity of the optical system.

It follows from Eq. (8) that, for constant responsivity and after R excluding the noise contribution, the power spectral density of photocurrent fluctuations is

$$S_I(f) = R^2 S_P(f).$$

If the spatial spectrum and the sensitivity kernel remain unchanged with distance, and only the fluctuation variance changes according to model (5), then in the linear approximation the power spectral density scales in proportion to that variance:

$$S_P(f \mid d) \propto \exp\left(-\frac{2d}{L_T}\right). \qquad (16)$$

This prediction is conditional. If the correlation scales, flow velocity, or optical sensitivity change with distance, the spectrum may change in shape as well as in amplitude.

3.4 Experimental data processing

Photocurrent spectra were calculated from selected informative time intervals in the WAV recordings. To make the estimates comparable, an FFT size of 1024, a Blackman–Harris window, and averaging of successive spectral estimates with 50% overlap were used. The informative intervals were identified from spectrograms. This procedure excludes portions in which the useful signal is absent or differs substantially from the operating regime.

The power in a specified frequency band is estimated using

$$P_{\text{band}} = \int_{f_1}^{f_2} S_P(f)\, df. \qquad (17)$$

To compare spectral shapes, the normalized power spectral density is used:

$$S_{\text{norm}}(f) = \frac{S_P(f)}{\int_{f_1}^{f_2} S_P(f)\, df}. \qquad (18)$$

The first quantity describes the integrated fluctuation power within the selected frequency band; the second describes how that power is distributed over frequency. This distinction is important. A decrease in absolute spectral power may reflect a reduction in fluctuation amplitude, whereas a change in normalized spectral shape may indicate changes in the spatial structure of the inhomogeneities, their transport velocity, or the optical sensitivity.

Reliable quantitative estimates require a consistent definition of the background spectrum and comparable informative intervals. Results obtained using preliminary choices of intervals and background segments are therefore considered diagnostic rather than final metrological measurements.

2.4. Experimental results

Spectra at different interaction-region positions along the optical path

Figures 2 and 3 show the averaged photocurrent spectra for the horizontal and vertical geometries at different interaction-region positions along the optical path, designated in the experiment as 0, 4, 8, and 12 m. These

values refer to the longitudinal position of the interaction region in the adopted coordinate system, not to the distance between the hair dryer and the laser beam.

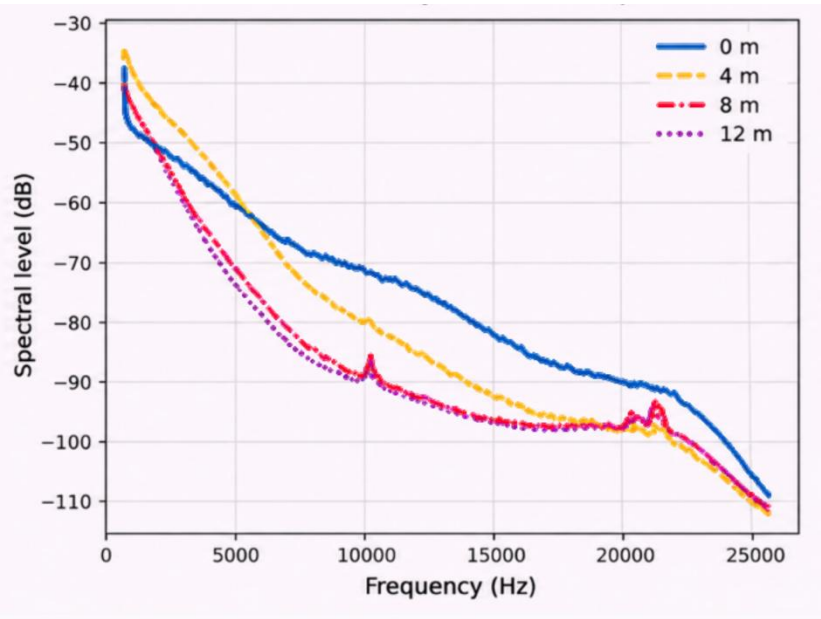


Figure 2. Time-averaged photocurrent spectra for the horizontal geometry at different interaction-region positions along the optical path.

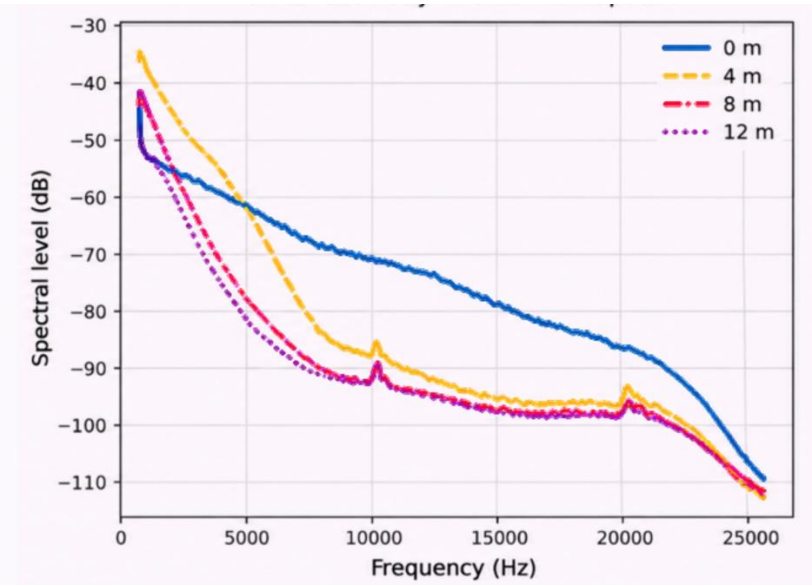


Figure 3. Time-averaged photocurrent spectra for the vertical geometry at different interaction-region positions along the optical path.

The spectral curves change shape as the interaction region is moved along the optical path, and the pattern of change differs between the horizontal and vertical geometries. A relative increase in low-frequency spectral power as the hair dryer is moved farther from the RRS is particularly noticeable in the vertical geometry.

Spectra as a function of distance from the hair dryer

Figures 4 and 5 show the averaged photocurrent spectra for the horizontal and vertical geometries at fan-to-beam distances d = 2, 5, 10, 25, and 40 cm, with z = 0 m. Figures 6 and 7 show the corresponding series for z = 8 m.

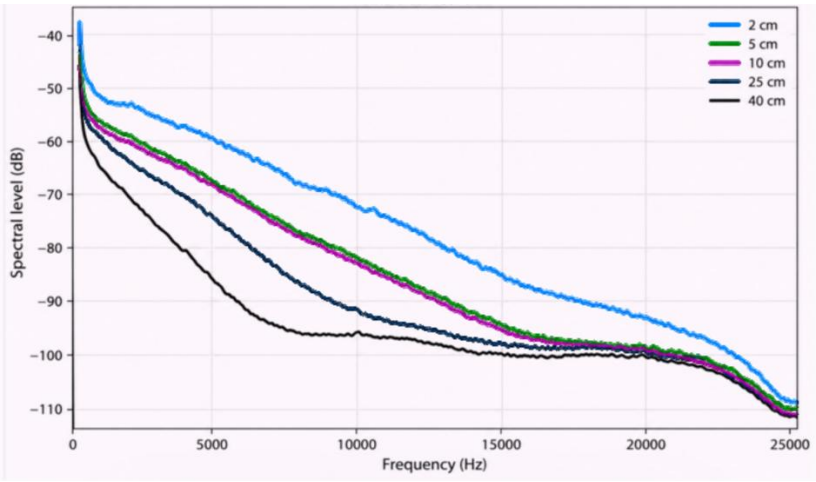


Figure 4. Time-averaged photocurrent spectra for the horizontal geometry at different fan–beam distances, with the interaction region at z = 0 m.

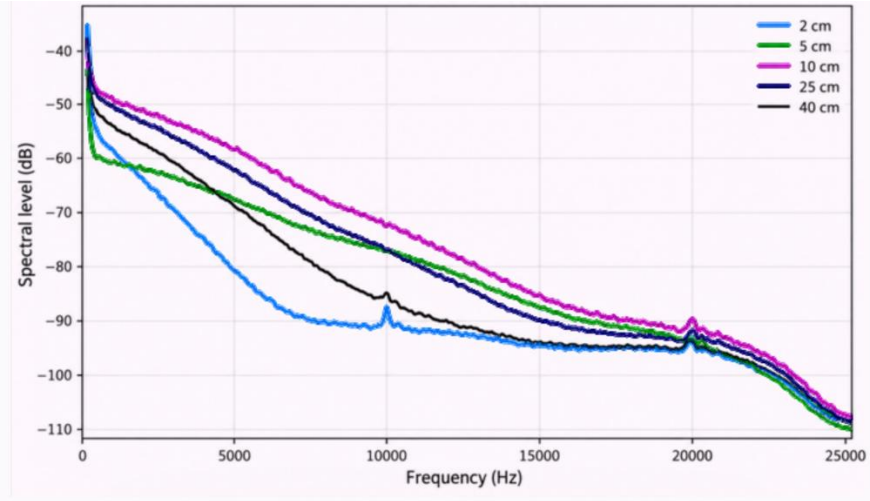


Figure 5. Time-averaged photocurrent spectra for the vertical geometry at different fan–beam distances, with the interaction region at z = 0 m.

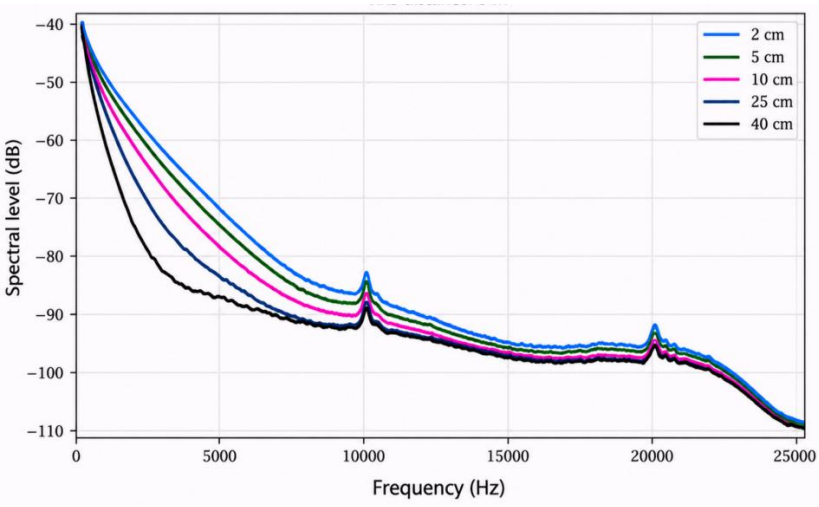


Figure 6. Time-averaged photocurrent spectra for the horizontal geometry at different fan–beam distances, with the interaction region at z = 8 m.

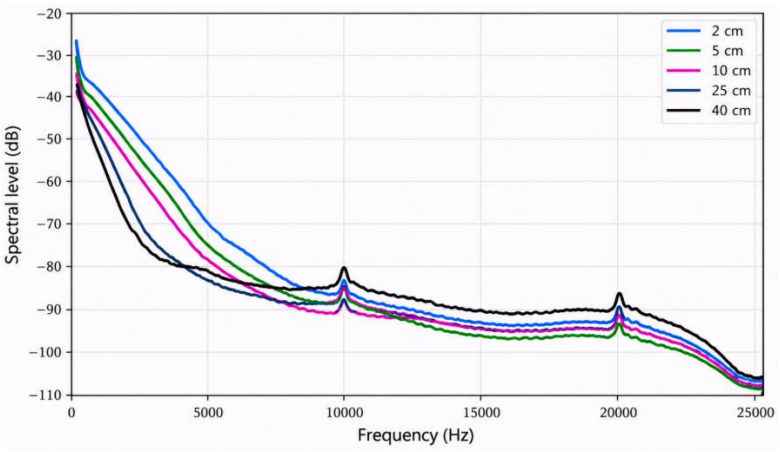


Figure 7. Time-averaged photocurrent spectra for the vertical geometry at different fan–beam distances, with the interaction region at z = 8 m.

In some series, the preliminary estimate of relative power decreases as the distance between the hair dryer and the laser beam increases. However, the spectral curves change in both level and shape, and some dependencies are non-monotonic. These results do not establish a universal monotonic decrease in the amplitude of temperature fluctuations.

The strongest non-monotonic behavior is observed in the vertical series at z = 0 m, where the preliminary power estimate reaches a maximum at d = 5 cm. Possible explanations include an actual change in the thermal-flow structure, a change in transport velocity, uncertainty in selecting the informative interval, and sensitivity to background correction. Overall, the experiments show that the signal depends on distance, but they do not establish a universal attenuation law.

Preliminary quantitative estimate of relative power

During preliminary processing, the relative fluctuation power in the 100 Hz–6 kHz band was calculated. For each series, the value at 2 cm was set to unity. An estimate of the background spectrum was subtracted from the spectrum of the informative segment, after which negative values of individual spectral components were set to zero before integration.

The results are summarized in Table 1.

Table 1. Preliminary relative power after background correction

Fan–beam distance	Vertical, z = 0 m	Vertical, z = 8 m	Horizontal, z = 0 m	Horizontal, z = 8 m
2 cm	1,000	1,000	1,000	1,000
5 cm	19,441	0,487	0,243	1,270
10 cm	11,946	0,755	0,250	0,917
25 cm	4,543	0,445	0,121	0,598
40 cm	0,949	0,082	0,019	0,342

The table is intended to identify trends and should not be treated as a quantitative validation of the model. In three of the four series, the relative power at some larger distances is lower than at 2 cm. This does not eliminate the pronounced non-monotonic behaviour in some series or the sensitivity of the estimates to the selected informative interval and background correction.

Dependence of the spectrum on the position of the interaction region

The spectral characteristics change when the nominal position of the interaction region along the optical path is

changed. This is consistent with the model because the sensitivity kernel depends on the propagation geometry and on the relative positions of the phase perturbations, the retroreflective surface, and the receiving aperture. However, these changes cannot be attributed to optical geometry alone: the statistical properties of the thermal flow may also vary along the path. Separating these effects requires additional measurements or independent estimates of the flow parameters.

Horizontal and vertical geometries

The horizontal and vertical series exhibit different spectral characteristics. These differences are consistent with possible anisotropy in the spatial correlation of temperature inhomogeneities. In the model, the temporal spectrum depends on the projection of the inhomogeneity spatial spectrum onto the transport direction. Consequently, rotating the flow relative to the optical system can change the spectral shape even when the fluctuation variance is unchanged.

Nevertheless, the observed differences do not constitute reliable proof of anisotropy. They may also be affected by differences in flow velocity, the mean temperature field, the position of the hair dryer, and uncertainty in identifying informative intervals. Quantifying anisotropy requires independent measurements of flow velocity, comparison of normalized spectra, and an assessment of measurement repeatability.

3. DISCUSSION

3.1. Agreement between the model and experimental observations

The main model predictions and the comparison with the experimental results are summarized in Table 2.

Table 2. Comparison of analytical predictions and experimental observations

Model prediction	Experimental observation	Degree of agreement and limitations
A decrease in the amplitude of temperature and associated phase fluctuations is expected to reduce absolute spectral power, all else being equal.	In several series, the overall spectral level decreases as the distance between the hair dryer and the laser beam increases. The dependence is not the same for all geometries and interaction-region positions.	Qualitative agreement in some series. Universal monotonic attenuation is not confirmed; the comparison depends on background correction and the selection of informative intervals.
If the fluctuation amplitude follows the proposed phenomenological exponential law, while the spatial structure and optical sensitivity remain unchanged, the absolute spectrum should scale in proportion to the fluctuation variance.	Preliminary relative-power estimates show non-monotonic dependencies and differences between series. Some values are particularly sensitive to the processing procedure.	Not quantitatively confirmed. The exponential law should be treated as a testable hypothesis, not as an established law of the thermal flow.
Changes in spatial correlation scales and/or transport velocity may change characteristic frequencies and the normalized spectral shape.	The spectra show differences in curve shape, including at low and intermediate frequencies; local features near 10 and 20 kHz are visible in some series.	Consistent with possible structural changes, but not proof of them. Identifying the cause requires background-spectrum checks, repeated recordings, and independent estimates of velocity or correlation

		scales.
For an anisotropic spatial structure, changing the transport direction relative to the optical system may cause differences between the spectral characteristics of the horizontal and vertical geometries.	The horizontal and vertical series have different spectral shapes and relative levels.	Qualitative agreement. The available spectra do not allow anisotropy of the thermal inhomogeneities to be separated unambiguously from differences in transport velocity and optical sensitivity.
The position of the interaction region along the path may change the measured spectrum through changes in the statistics of the inhomogeneities and/or in the optical sensitivity kernel.	The spectra differ for nominal interaction-region positions z = 0, 4, 8, and 12 m.	The dependence is supported by observations. The specific mechanism has not been established because the thermal-flow statistics and optical sensitivity were not measured separately.
In a two-pass arrangement, the response depends on the combined contributions of the forward and return passes and on the correlation of phase perturbations along their respective paths.	The setup uses forward and return optical paths, but the spectra alone do not isolate the contribution of each pass.	Included physically in the analytical model but not quantitatively verified. Verification requires a justified calculation of the sensitivity kernel accounting for the geometry of both passes.

Overall, the experimental results support the general physical picture of signal formation, but they do not establish all of the model parameters.

3.2. Separating amplitude and structural effects

An important next step is to distinguish between two effects. The first is a reduction in the overall fluctuation intensity, which, in the linear approximation, reduces absolute spectral power. The second is a change in the spatial structure of the inhomogeneities, which may alter the normalized spectral shape and characteristic frequencies. If normalized spectra measured at different distances nearly coincide, this would be consistent with a predominant change in fluctuation amplitude. If the spectral shape changes systematically, changes in correlation scales, transport velocity, or optical sensitivity must also be considered.

The available plots suggest that both effects may be present, but they cannot yet be separated conclusively. Doing so requires checking the background correction and the repeatability of the spectral shapes.

3.3. Model limitations

The proposed model uses several approximations.

First, the spatial correlation is represented by a Gaussian function with two transverse scales. The actual structure of the thermal plume may be more complex.

Second, the frozen-transport hypothesis assumes that the inhomogeneities are advected by the flow faster than they evolve. For a real thermal flow, this approximation is valid only over a limited range of time scales [3, 4].

Third, the linear power response assumes weak phase perturbations. For larger perturbations, nonlinear terms may become significant.

Fourth, the exponential attenuation law is introduced as an initial model rather than as a known universal law of thermal convection.

Finally, the two-pass sensitivity kernel has not been fully validated quantitatively. The contribution of optical geometry therefore cannot yet be conclusively separated from changes in the statistical properties of the thermal flow.

3.4. Limitations of the experimental interpretation

The informative intervals were selected from spectrograms, but their boundaries remain uncertain for some recordings. In addition, the preliminary background-power estimate can strongly affect the result when the useful signal is weak. The relative-power values in Table 1 should therefore be treated as diagnostic: they indicate possible trends but are not sufficiently accurate to determine attenuation parameters.

CONCLUSION

An analytical model for laser detection of thermal flows has been proposed, linking the statistics of refractive-index fluctuations in air to the measured photocurrent spectrum. The model accounts for the two-pass optical geometry, the lateral offset of the photodetector, the finite receiving aperture, anisotropy in the spatial correlation of the inhomogeneities, and possible attenuation of their intensity with distance from the heat source.

Experiments using a hair dryer as the thermal-flow source investigated horizontal and vertical geometries, different distances between the hair dryer and the laser beam, and different positions of the interaction region along the optical path.

For the series investigated, the photocurrent spectra depend on both the distance between the hair dryer and the laser beam and the experimental geometry. The horizontal and vertical series exhibit different spectral shapes, and the preliminary estimates of relative power show non-monotonic dependencies. These observations are consistent with the signal being affected by fluctuation amplitude, spatial structure, and the optical sensitivity of the setup; they do not identify any one mechanism uniquely.

However, the non-monotonic behavior of some dependencies, uncertainty in the boundaries of certain informative intervals, and the lack of independent measurements of flow parameters mean that neither the exponential attenuation law nor the correlation-cell dimensions can be considered quantitatively established.

The principal contribution of this work is the formulation of an analytical model connecting the spatiotemporal properties of refractive-index fluctuations, the two-pass geometry of the optical system, and the integrated photocurrent spectrum, together with preliminary experimental observations that are qualitatively consistent with some of the mechanisms included in the model.

Future work should focus on testing the repeatability of the spectral dependencies, refining background correction, and determining the thermal-flow parameters quantitatively.

REFERENCES

1. Drain, L. E. The Laser Doppler Technique. Chichester: John Wiley & Sons, 1980. ISBN 0-471-27627-8.
2. Tropea, C. Laser Doppler anemometry: recent developments and future challenges. Measurement Science and Technology, 6, 605–619 (1995). DOI: 10.1088/0957-0233/6/6/001.
3. Li Jiwei, Luo Kai, Shang Jiahao, Wang Yejun, Wang Qiu, Zhao Wei. Research progress of laser diagnostics for velocimetry in hypersonic flows. Chinese Journal of Theoretical and Applied Mechanics, 2024, 56(4): 890-914.DOI: 10.6052/0459-1879-23-242
4. Evans MJ and Medwell PR (2019) Understanding and Interpreting Laser Diagnostics in Flames: A Review of Experimental Measurement Techniques. Front. Mech. Eng. 5:65. DOI: 10.3389/fmech.2019.00065
5. Andrews L. C., Phillips R. L. Laser Beam Propagation through Random Media. 2nd ed. Bellingham, WA: SPIE Press, 2005.

6. Pérez D. G., Farfán-Bachiloglu H., Sepúlveda M. Spatiotemporal statistics of optical turbulence beyond Taylor's frozen turbulence hypothesis. Journal of the Optical Society of America A. 2024. Vol. 41, No. 6. P. B135–B143. DOI: 10.1364/JOSAA.520550.
7. Schock M., Spillar E. J. Method for a quantitative investigation of the frozen flow hypothesis. Journal of the Optical Society of America A. 2000. Vol. 17, No. 9. P. 1650–1658. DOI: 10.1364/JOSAA.17.001650.
8. G.N. Dolya, E.S. Litvinova. Retroreflective laser detector of acoustic oscillations// Proceedings of 12th International Conference on Laser & Fiber-Optical Networks Modeling (LFNM'2016), Sept.15-18, Odessa, Ukraine. P.108-111 DOI: 10.1109/LFNM.2016.7851212
9. Dolya G.N., Katunin A.N, Sadovy K.V., Chudovskaja E.S. Laser radiation parameters at detection of decay and fire sources. / Proceedings of 4-th International Conference on Advanced Optoelectronics and Lasers. Alushta, Crimea, 2008, p.351-353